[redacted] CONFIDENTIAL

NACA

RESEARCH MEMORANDUM

LIMITED HEAT-TRANSFER, DRAG, AND STABILITY RESULTS FROM AN INVESTIGATION AT MACH NUMBERS UP TO 9 OF A LARGE ROCKET-PROPELLED 10° CONE

By James R. Hall and Katherine C. Speegle

Langley Aeronautical Laboratory
Langley Field, Va.

NATIONAL ADVISORY COMMITTEE
FOR AERONAUTICS

WASHINGTON

July 22, 1957

[redacted]

NACA RM L57E08

NATIONAL ADVISORY COMMITTEE FOR AERONAUTICS

RESEARCH MEMORANDUM

LIMITED HEAT-TRANSFER, DRAG, AND STABILITY RESULTS FROM AN INVESTIGATION AT MACH NUMBERS UP TO 9 OF A LARGE ROCKET-PROPELLED 10° CONE

By James R. Hall and Katherine C. Speegle

SUMMARY

Limited information on the heat transfer, drag, and stability of a large rocket-propelled 10° cone has been obtained in a flight test by Langley Pilotless Aircraft Research Division. Turbulent flow was indicated at the most forward temperature measuring station at local Reynolds numbers from 1.6×10^6 to 23×10^6 and corresponding Mach numbers of 0.6 to 2.15. The measured drag coefficient at a Mach number of approximately 9.0 was about midway between theoretical predictions for laminar and turbulent skin friction. The average Reynolds number at the time of the drag measurement was 10.4×10^6. A single determination was made of the static stability and damping constant during thrust at a Mach number of 5.2.

INTRODUCTION

Delay of transition to Reynolds numbers of about 21×10^6 (based on free-stream conditions) on highly polished cones has been reported in references 1 and 2. Tip blunting employed in the cone of reference 2 contributed to the delay of transition by reducing the local Reynolds number in the region enveloping the boundary layer. The present test on a large blunted 10° cone with superpolished surface was designed to obtain heating measurements at high Reynolds numbers and Mach numbers. In addition, measurements were made of drag and stability.

Because of a partial instrumentation failure it was possible to obtain a temperature history only at Mach numbers from 2.1 to 0.6 and a single determination of static stability and damping constant at a Mach number of 5.2 during the thrusting portion of the flight and drag measurements at a Mach number of 9. These limited results are presented

in view of the dearth of experimental aerodynamic heating data at all Mach numbers and stability parameters at hypersonic Mach numbers.

SYMBOLS

a_l	longitudinal acceleration, g units
d	diameter of model (used as reference length for moment coefficient), 1.5 ft
c_p	specific heat of air, Btu/lb-°F
$c_{p,w}$	specific heat of wall, Btu/lb-°F
C_D	drag coefficient, Drag/qS
N_{St}	Stanton number, $h/\rho c_p V$
C_N	normal-force coefficient, Normal force/qS
C_Y	transverse-force coefficient, Transverse force/qS
C_R	resultant-force coefficient, $\sqrt{C_N^2 + C_Y^2}$
C_{m_α}	slope of pitching-moment curve (criterion of static stability)
h	heat-transfer coefficient, $\frac{\tau_w \rho_w c_{p,w} \frac{dT_w}{dt}}{T_{aw} - T_w}$
I	moment of inertia of model in pitch and yaw, 39.5 slug-ft^2
M_∞	free-stream Mach number
N_{Pr}	Prandtl number
q	dynamic pressure, lb/sq ft
$R_{\infty,l}$	free-stream Reynolds number based on length of 1 foot
S	base area, 1.77 sq ft

T	thrust, lb
T_{aw}	adiabatic wall temperature, $^{\circ}R$
T_{so}	stagnation temperature, $^{\circ}R$
T_v	local temperature of air just outside boundary layer, $^{\circ}R$
T_w	temperature of wall, $^{\circ}R$
t	time, sec
V	velocity, ft/sec
W	weight, lb
ρ_w	density of wall, slug/cu ft
τ_o	total damping constant based on time for oscillation to damp to half amplitude, $\frac{1}{2} \log_e \left(C_{R,max}^2 - C_{R,min}^2 \right)$, 1/sec
θ	flight-path angle from horizontal, deg
ρ	density of air, slug/cu ft
τ_w	thickness of wall, ft
ω_o	frequency of resultant-force coefficient, 2π/Period, radians/sec

MODEL, INSTRUMENTATION, AND TEST PROCEDURE

Model

The test vehicle was a 5° semiangle cone of length of 103 inches, and a base diameter of 18.0 inches. The nose tip was blunted to a 3/4-inch-diameter hemisphere. Figure 1 shows the construction and internal arrangement of the test vehicle. The outer skin of the cone was fabricated from 1/32-inch Inconel except for the nose tip, which was heavier. A layer of balsa wood of thickness varying from about 1/4 inch to 3 inches separated the outer skin from the internal structure. The internal structure consisted of ballast, telemeter, and rocket motor. The ballast and telemeter were enclosed in a 1/32-inch stainless-steel radiation shield.

[redacted]

Telemeter components were protected by additional shielding over individual components. The forward 55 inches of the cone and a triangular segment extending rearward over the main line of thermocouples were highly polished. The triangular segment was employed in order to include an extra thermocouple in the polished region with a minimum of polishing effort. A finish of 2 microinches existed over the first foot of length, and gradually increased to 5 microinches at the rear of the polished portion. No scratches were apparent in the surface, which had the appearance of a mirror. The polishing operation was accomplished manually by using diamond-dust abrasives. The finish was measured by an interference microscope which had an accuracy of about 1 microinch. The high polish was superimposed on a random waviness of up to 0.01 inch which existed in the skin due to fabrication prior to the polishing operation. The polished skin was protected with a strippable plastic coating until installed on the launcher. Thereafter a paper wrapper protected the finish from contamination by sand or salt water until blown away at take-off.

Instrumentation

The model carried a standard NACA six-channel telemeter which was protected from aerodynamic heating by a radiation shield and individual covers over the telemeter components. Temperatures were measured by 12 thermocouples welded to the inside of the skin at the locations shown in figure 1. Accelerations were measured with accelerometers of the following ranges:

Thrust acceleration, g units	1 to 55
Drag acceleration, g units	1 to -10
Normal acceleration, g units	±6
Transverse acceleration, g units	±6

Velocity was measured by means of a CW Doppler velocimeter and space position was measured by an NACA modified SCR-584 radar set. Atmospheric conditions and wind velocity aloft were measured by means of Rawin set AN/GMD-1A released at the time of launching.

Free-Flight Test

The propulsion system employed in this experiment was a 3-stage arrangement of M6 JATO (Honest John), M5 JATO (Nike booster), and JATO 6KS-3000, T40 rocket motors. The general arrangement and relative size of the components are shown in a photograph of the test vehicle on the launcher (fig. 2). The Honest John accelerated the combination to a Mach number of 2.15 in 5.0 seconds. At burnout of the Honest John, stages two and three (which were locked together) separated

from the first stage due to the relative weight-drag ratio. After a coast period of 40 seconds during which the combination decelerated to a Mach number of 0.6, the second stage was fired, accelerating the combination to a Mach number of 5.0. Then, after a coast period of 1.5 seconds the final stage was fired, further accelerating the model to a Mach number of 8.97. A frangible diaphragm supporting a segmented ring, to which stages two and three were screwed, held them together until the diaphragm was blown out by the rocket blast from stage three. The last two stages were fired by means of a mechanical timer which simultaneously fired a delay squib in the third-stage-rocket motor and an instantaneous squib in the second-stage-rocket motor.

The data-producing portion of the trajectory followed by the model is shown in figure 3. The velocity time history is shown in figure 4. The velocity was obtained by three independent methods which agree very well: (1) direct measurement was made by Doppler velocimeter until the test vehicle exceeded the range of the instrument; (2) the space position reported by SCR-584 radar was differentiated to obtain velocity; and (3) the measurement of longitudinal acceleration was employed to obtain velocity by an integration procedure. It was necessary to correct the drag accelerometer measurements by the constant factor 0.64g in order to force agreement of the integrated velocity with the very accurate Doppler velocimeter measurements. Beyond the range of this instrument the velocities obtained from integrated accelerometer and differentiated position measurements agree very well. Figure 5 shows the variation of atmospheric conditions with altitude as measured by the Rawin apparatus. Standard conditions (ref. 5) were assumed above 64,000 feet due to lack of measured data above that altitude. Free-stream Mach number and Reynolds number based on a length of 1 foot are presented in figure 6.

Helium-Gun Tests

The 6-inch helium gun at the Langley Pilotless Aircraft Research Station at Wallops Island, Va., was employed in preliminary 1/10-scale tests of drag and stability of 10° cones. The operation of this facility is described in reference 3. Three 1/10-scale models were flown with center-of-gravity locations at 61.7, 64.3, and 66.0 percent of the total length. The drag was obtained from Doppler velocimeter measurements by the method described in reference 4. An indication that the models were statically stable was also obtained from the velocity record in that instability would be reflected in an excessively low or erratic velocity.

[redacted]

ACCURACY

The telemetered measurements are generally considered to be accurate within ±2 percent of full-scale range. This represents the maximum error in the absolute level of the measurements in the absence of undetected zero shifts. The relative error is much smaller as is evidenced by the scatter of the measured data. In the case of the temperature measurements the possible absolute and relative errors were ±24° F and ±10° F, respectively. The random scatter apparent in the measurement of normal and transverse acceleration was 0.04g which represents 0.33 percent of the maximum acceleration measured by these instruments. The thrust and drag accelerometers suffered zero shifts after launching. In both cases, however, it was possible to make corrections by relating the shifted measurements to the velocity obtained from Doppler velocimeter and position radar measurements. The thrust accelerometer measured almost full-scale deflection during the periods of acceleration so that the maximum error in the measurement would be 2 percent of the indicated value. A comparable value for the drag measurements is of the order of 15 percent due to the smaller percentage of available range utilized. The random error in drag is indicated to be about 5 percent. Based on the basic measurements, it is estimated that C_{m_α} and the damping constant are correct within ±5 percent.

RESULTS AND DISCUSSION

T40 Performance

The thrust of the T40 rocket motor in the last stage was computed from the expression

$$\text{Thrust} = W\left(a_l + \sin\theta\right) + C_D qS$$

The computed thrust is compared in figure 7 with the measured thrust of a T40 motor made during a ground test with a standard 5-inch nozzle and with the thrust predicted on the basis of this result for a motor with a 10-inch nozzle for the pressure condition corresponding to the trajectory of the model used in the present investigation. As shown by figure 7, the measured in-flight performance was about 6 percent better than predicted for this rocket motor.

Temperature

Temperature measurements were available only during the relatively low-speed period between 0 and 45 seconds. The temperature measurements taken during this period showed no variation with length along the entire cone, although turbulent theory predicts a maximum difference of about 25° between the foremost and rearmost thermocouples. The measured variation of temperature with time is shown in figure 8. The measured temperature points are shown to indicate the amount of scatter in the measurements. The theoretical termperature variation at stations 21.5 and 100.4 for turbulent flow and at station 21.5 for laminar flow are also shown. These temperatures were obtained by a step-by-step computation using the expression

$$\Delta T_w = \frac{\left(N_{St}\rho V c_p\right)_v}{\rho_w c_{p,w} \tau_w} \left[T_{aw} - T_w\right] \Delta t$$

where

$$T_{aw} = \text{Recovery factor} \left(T_{so} - T_v\right) + T_v$$

The value of N_{St} was given by Van Driest in reference 6 and recovery factors equivalent to $N_{Pr}^{1/2}$ and $N_{Pr}^{1/3}$ were used for the laminar and turbulent calculations, respectively. The length of turbulent flow was calculated from the nose tip. Zero temperature lag was assumed throughout the skin. Comparison of the level and slope of the measured temperatures with theoretical temperatures indicates that turbulent flow prevailed during the entire period, during which time the free-stream Reynolds number based on a length of 1 foot decreased from 12.4×10^6 to 0.75×10^6. The turbulent flow experienced is predicted by the two-dimensional theory of reference 7, which defines a boundary of T_w/T_v and Mach number necessary to achieve complete laminar boundary-layer stability. The ratio T_w/T_v for this flight never enters the infinite stability region, even if blunt tip conditions of local temperature and Mach number are used. Blunt tip conditions were calculated by assuming a normal-shock total-pressure loss and that surface static pressure was unaffected by bluntness. The 10° cones reported in references 8 and 9 retained laminar flow at Reynolds numbers up to 33.1×10^6. However, the surface roughness, Mach number, wall temperature ratio, and tip bluntness were different than in the present case, and, consequently, direct comparisons are meaningless.

Stability

During stage-three firing the normal and transverse accelerometers revealed that a damped oscillation occurred, upon which a roll was superposed. The theory of reference 10 was used to obtain the static stability and damping of the cone while undergoing thrust. The procedure followed in applying the method is outlined in some detail since this is one of the first applications reported for the method. The Mach number at the midpoint of the oscillation that was analyzed was 5.25. The magnitude of the oscillation was about 1°. Although the weight and moment of inertia were changing continually, their values at the midpoint of the damped oscillation were estimated by assuming a linear variation between the known values before and after rocket-motor burning. The normal and transverse oscillations of the model converted to force coefficients are shown in figure 9. It can be seen that coupling exists between the two modes of motion. Normal- and transverse-force coefficients were then plotted against each other as shown in figure 10. The constancy of roll rate is shown by the constant angle between the peaks of successive loops of the plot. By using the trim center estimated from this figure, a plot was made of the square of the resultant-force coefficient about the trim center (fig. 11). Small corrections to the time scale were made to compensate for the density change with time as indicated in reference 10. The resulting oscillation was then used to evaluate the static stability C_{m_α} by employing the relationship

$$C_{m_\alpha} = \frac{I}{qSd}\left(\omega_o^2\right) = -1.137$$

This value compares with the theoretical value of C_{m_α} of 0.86 computed in reference 11 by using Newtonian theory. Reference 11 does not consider the effect of longitudinal force on the static stability. Reference 12 derives a more complete expression for static stability which includes a longitudinal-force term, from which it can be seen that C_{m_α} during thrust should be higher than when the motor is not undergoing thrust. Although this correction is usually small, it would tend to improve the agreement between theory and experiment.

The damping constant τ_o was evaluated from the slope of a plot of $\frac{1}{2}\log_e\left(C_{R,max}^2 - C_{R,min}^2\right)$. This curve was not linear but increased in slope with time. The initial damping constant was calculated to be -0.407 and the final damping constant was -1.28. The corresponding magnitudes of oscillation were about 1.5° and 1.0°, respectively. The large change in damping over such a small range of angle of attack is inexplainable. These experimental values compare with the theoretical value of -0.464 for a 10° cone not undergoing thrust given by the Newtonian theory of reference 11. Hence, theory appears to agree better

[redacted]

with the initial measured value. Consideration of the effect of thrust as given by reference 12 would tend to increase the theoretical value and move it closer to the final measured value. The effect of the rocket-motor jet on the damping of the cone is negligible, according to the theory of reference 13.

Drag Coefficient

Free-flight tests.- The drag coefficients of the combination of stages two and three measured during the coast periods from Mach numbers of 1.2 to 2.4 and approximately 5.0 are compared in figure 12 with theoretical predictions. Agreement is good at the lower Mach numbers but the prediction is 20 percent higher at Mach number 5.0.

The drag coefficient of stage three is compared with theory for both laminar and turbulent skin friction in figure 13 for Mach numbers from 8.9 to 8.4. The measured drag coefficient is seen to lie about midway between the laminar and turbulent predictions. This implies that transition occurred at about the 3/4-length station, although the accuracy of the drag measurements is not sufficient to permit a definite statement.

Helium-gun tests.- The average drag coefficient measured in three 1/10-scale helium-gun tests at transonic speeds is compared with theory in figure 14. The measured points for the three tests are shown to indicate the amount of scatter in the measurements. Predicted drag coefficient is only about 75 percent of measured drag coefficient. The velocity measurements indicated that all three models were stable, including the one with center of gravity at the 2/3-length station for which theory predicts neutral stability. This hypothesis is based on the reasonable assumption that static instability would result in flight-path divergence which would cause the velocity data to be very erratic and contain a large abrupt decrease.

CONCLUSIONS

The results of the flight test of the large 5° semiangle cone described herein indicate the following conclusions:

1. Measurements indicated that turbulent flow prevailed at the most forward temperature measuring station at local Reynolds numbers from 1.6×10^6 to 23×10^6 corresponding to Mach numbers from 0.6 to 2.15.

2. Static stability measured at a Mach number of 5.2 while thrusting was about 30 percent higher than predicted by the Newtonian theory of

[redacted]

NACA Technical Note 3788 for constant velocities. Measured exponential damping constant varied from a value approximately equal to the theoretical value to a value approximately 3 times the theoretical value.

3. The measured drag coefficient at a Mach number of approximately 9.0 was about midway between theoretical predictions for laminar and turbulent skin friction.

Langley Aeronautical Laboratory,
National Advisory Committee for Aeronautics,
Langley Field, Va., April 12, 1957.

REFERENCES

1. Rabb, Leonard, and Disher, John H.: Boundary-Layer Transition at High Reynolds Numbers As Obtained in Flight of a 20° Cone-Cylinder With Wall to Local Stream Temperature Ratios Near 1.0. NACA RM E55I15, 1955.

2. Disher, John H., and Rabb, Leonard: Observation of Laminar Flow on a Blunted 15° Cone-Cylinder in Free Flight at High Reynolds Numbers and Free-Stream Mach Numbers to 8.17. NACA RM E56G23, 1956.

3. Hall, James Rudyard: Comparison of Free-Flight Measurements of the Zero-Lift Drag Rise of Six Airplane Configurations and Their Equivalent Bodies of Revolution at Transonic Speeds. NACA RM L53J21a, 1954.

4. Wallskog, Harvey A., and Hart, Roger G.: Investigation of the Drag of Blunt-Nosed Bodies of Revolution in Free Flight at Mach Numbers From 0.6 to 2.3. NACA RM L53D14a, 1953.

5. Anon.: Manual of ICAO Standard Atmosphere - Calculations by the NACA. NACA TN 3182, 1954.

6. Van Driest, E. R.: The Problem of Aerodynamic Heating. Aero. Eng. Rev., vol. 15, no. 10, Oct. 1956, pp. 26-41.

7. Van Driest, E. R.: Calculation of the Stability of the Laminar Boundary Layer in a Compressible Fluid on a Flat Plate With Heat Transfer. Jour. Aero. Sci., Dec. 1952, pp. 801-812.

8. Merlet, Charles F., and Rumsey, Charles B.: Supersonic Free-Flight Measurement of Heat Transfer and Transition on a 10° Cone Having a Low Temperature Ratio. NACA RM L56L10, 1957.

9. Rumsey, Charles B., and Lee, Dorothy B.: Measurements of Aerodynamic Heat Transfer and Boundary-Layer Transition on a 10° Cone in Free Flight at Supersonic Mach Numbers Up to 5.9. NACA RM L56B07, 1956.

10. Nelson, Robert L.: The Motions of Rolling Symmetrical Missiles Referred to a Body-Axis System. NACA TN 3737, 1956.

11. Tobak, Murray, and Wehrend, William R.: Stability Derivatives of Cones at Supersonic Speeds. NACA TN 3788, 1956.

12. Seiff, Alvin, Sommer, Simon C., and Canning, Thomas N.: Some Experiments at High Supersonic Speeds on the Aerodynamic and Boundary-Layer Transition Characteristics of High-Drag Bodies of Revolution. NACA RM A56I05, 1957.

13. Barton, M. V.: The Effect of Variation of Mass on the Dynamic Stability of Jet-Propelled Missiles. Jour. Aero. Sci., vol. 17, no. 4, Apr. 1950, pp. 197-203.

[redacted]

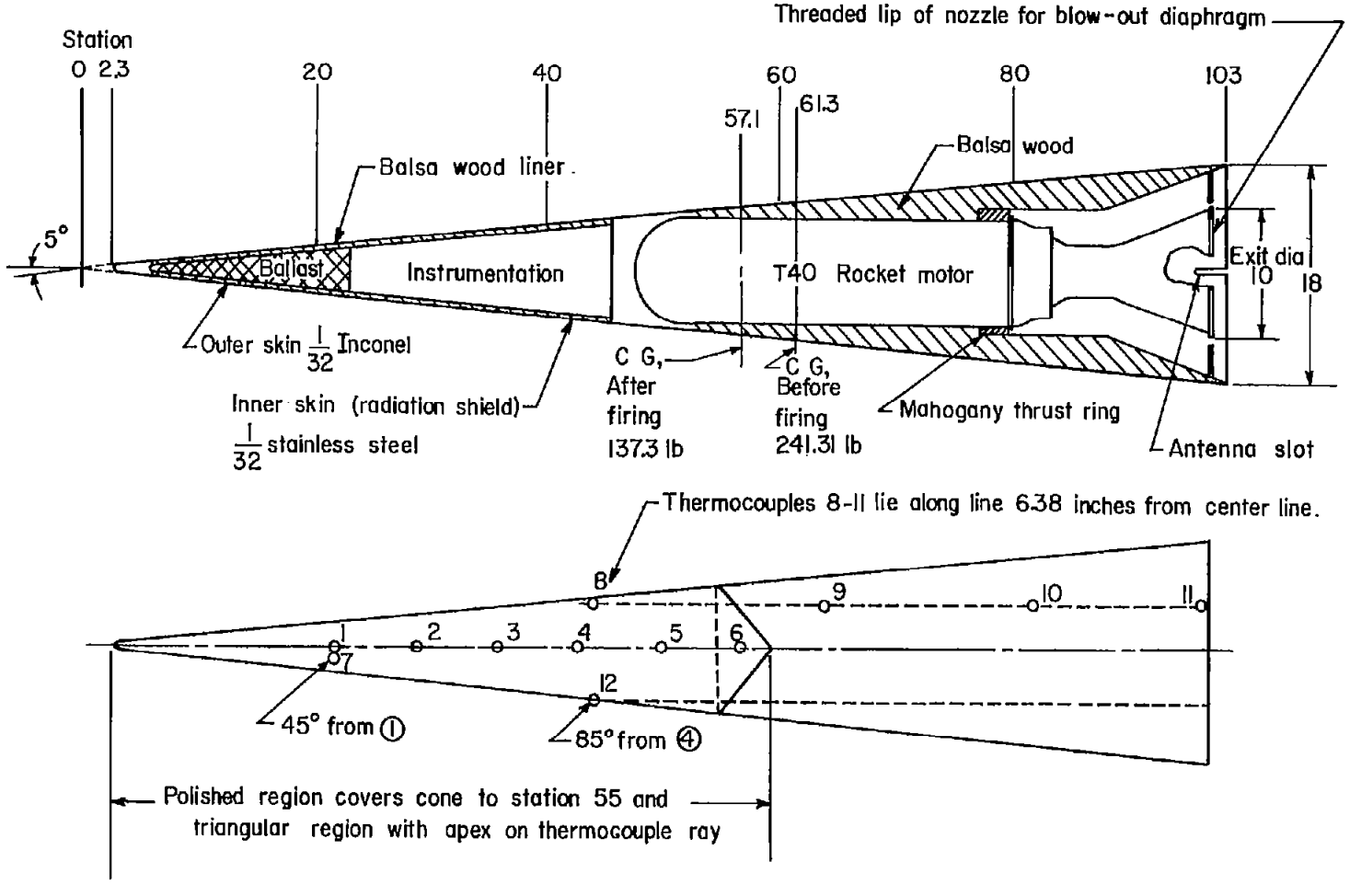

Figure 1.- Sketch of model and detail of nose construction. All dimensions are in inches.

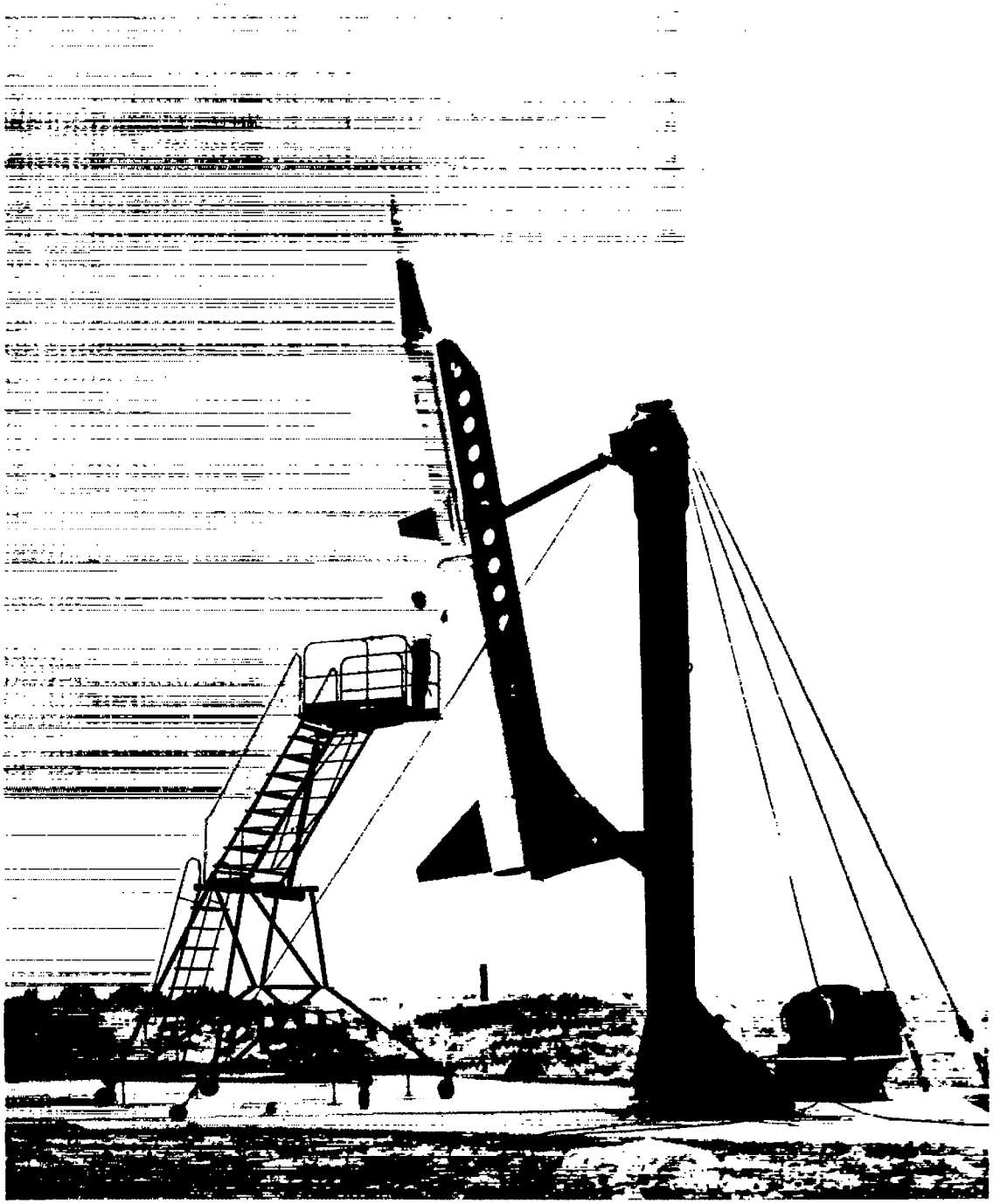

Figure 2.- Photograph of model and boosters on launcher. L-94542

[redacted]

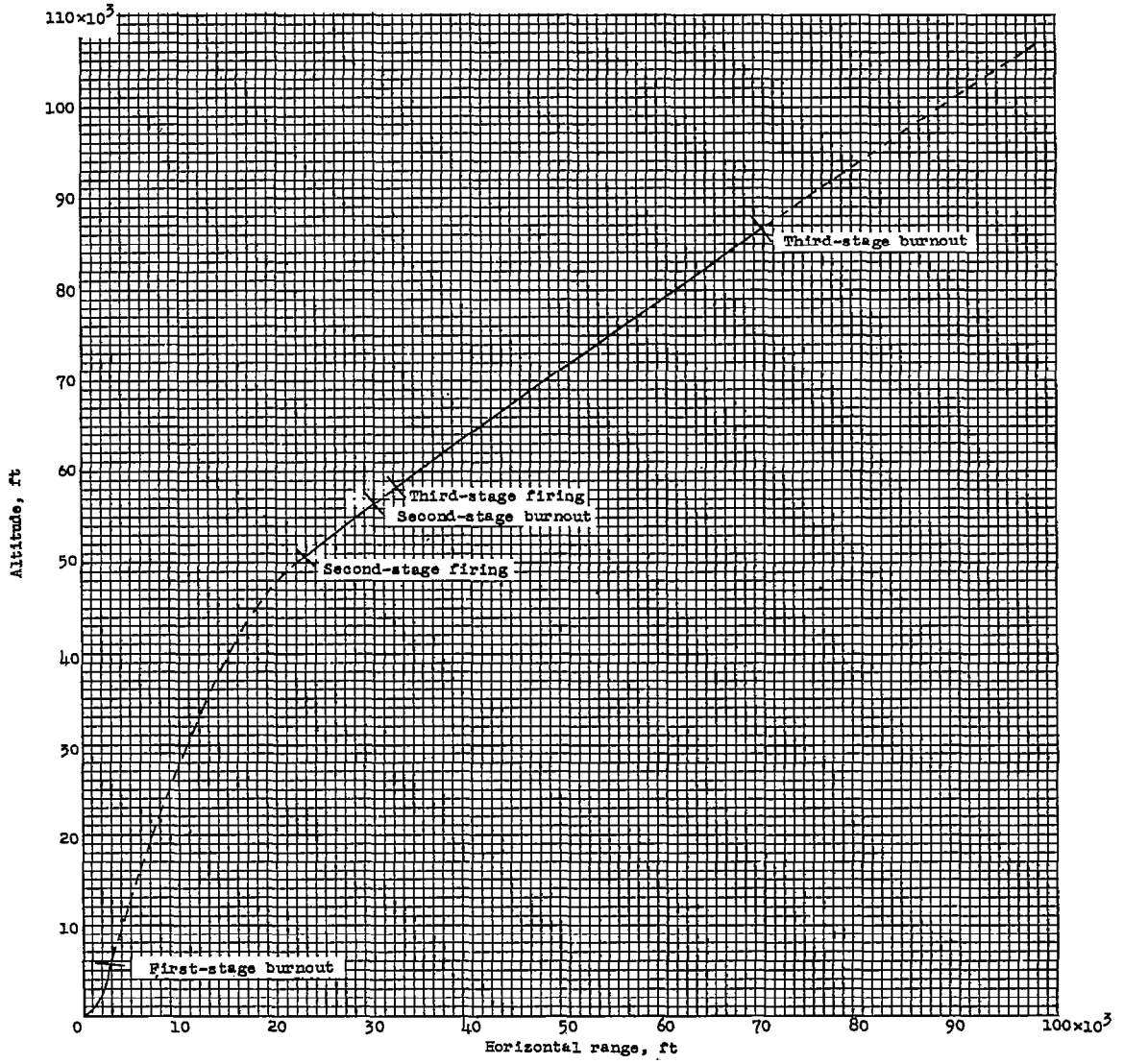

Figure 3.- A portion of trajectory followed by model.

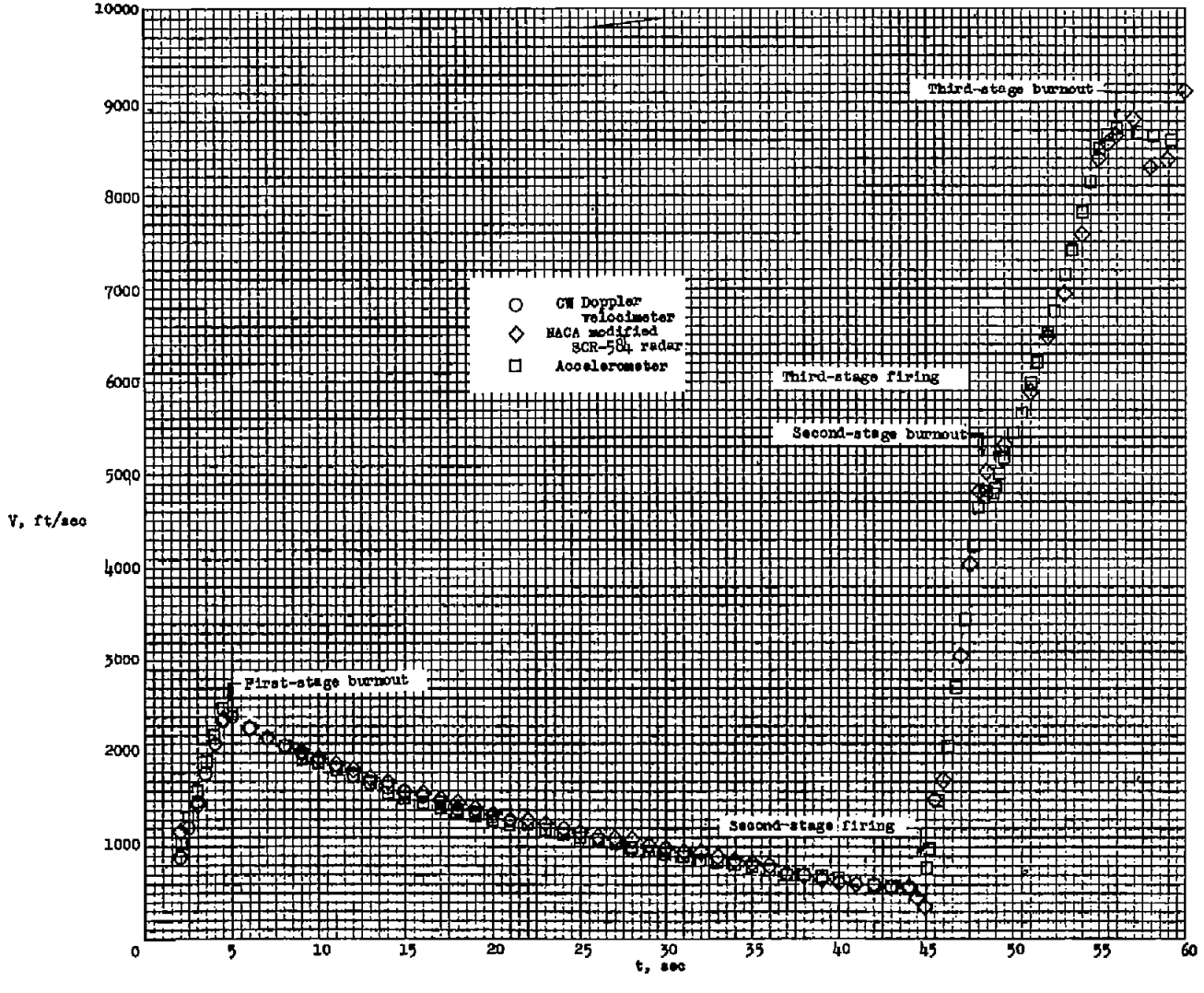

Figure 4.- Time history of model velocity.

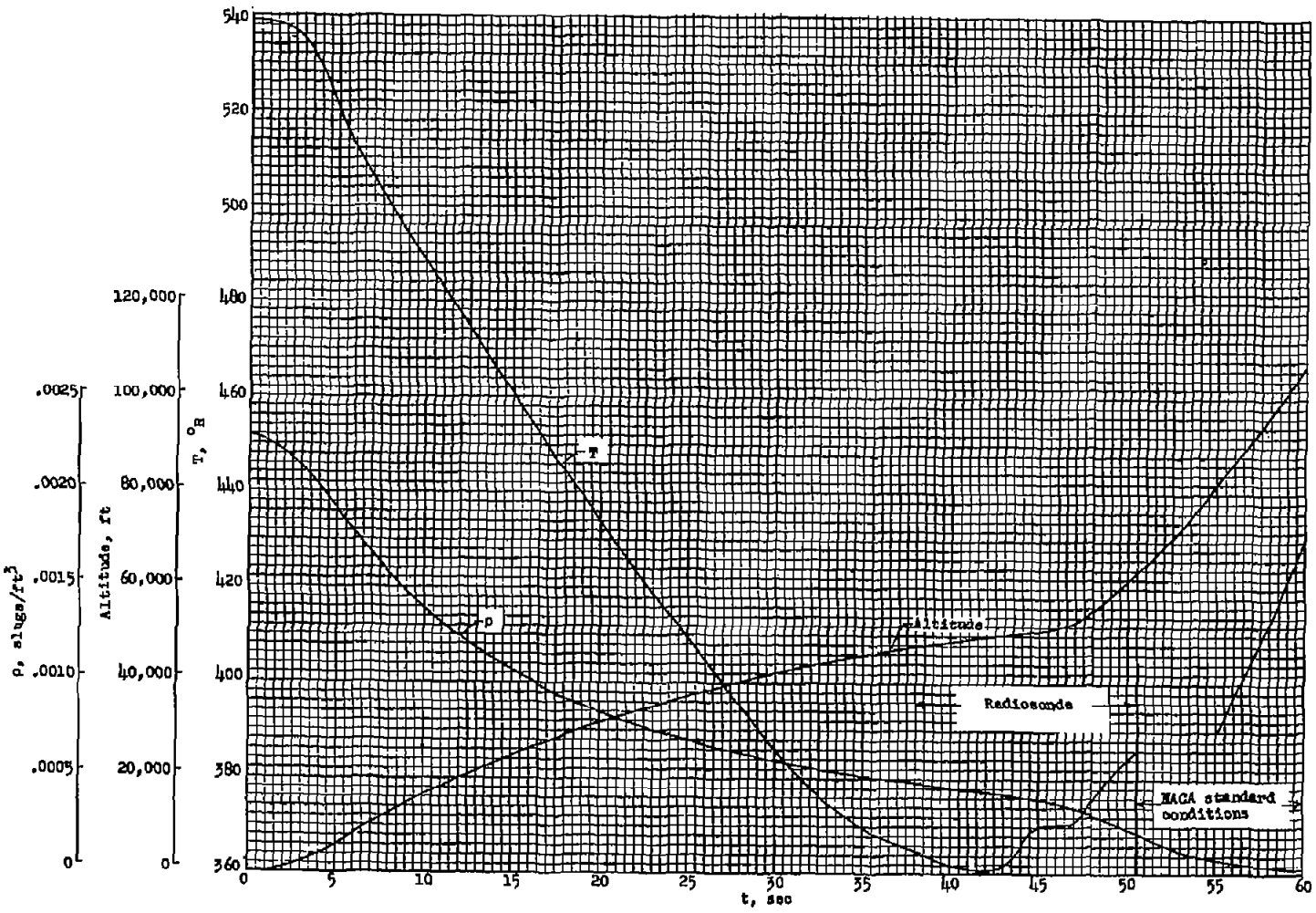

Figure 5.- Time history of model altitude, free-stream temperature, and density.

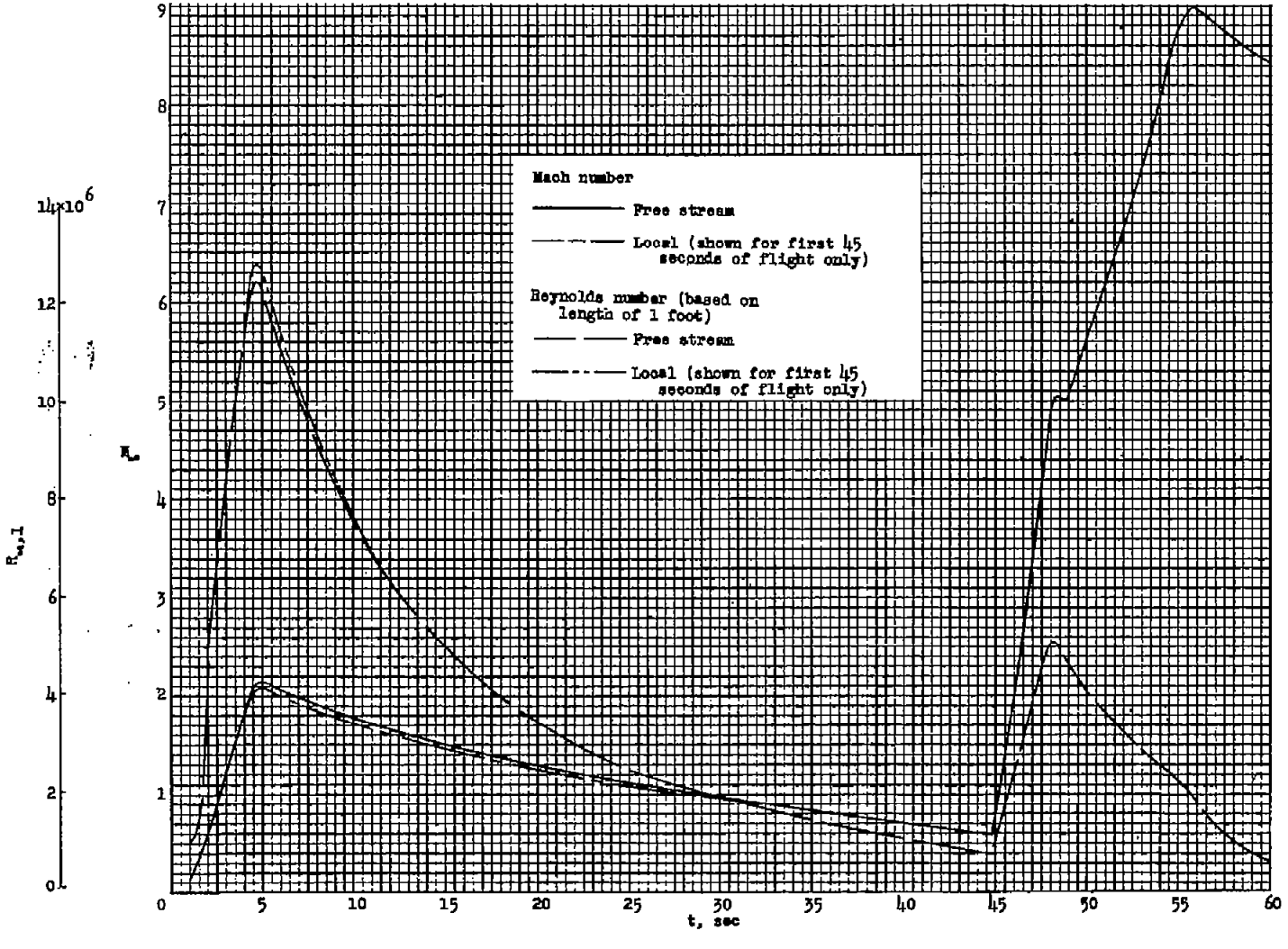

Figure 6.- Time histories of local and free-stream Mach number and Reynolds number based on length of 1 foot. Local conditions are for sharp cone.

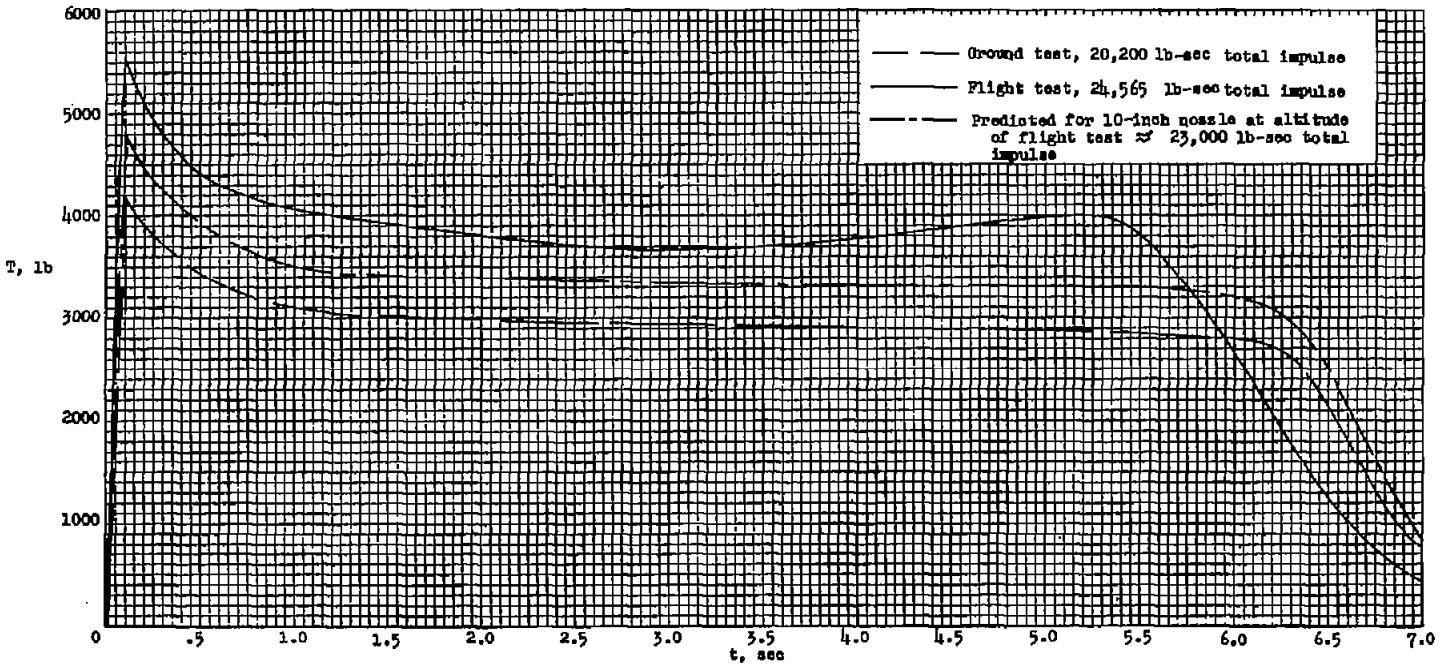

Figure 7.- Performance of T40 rocket motor.

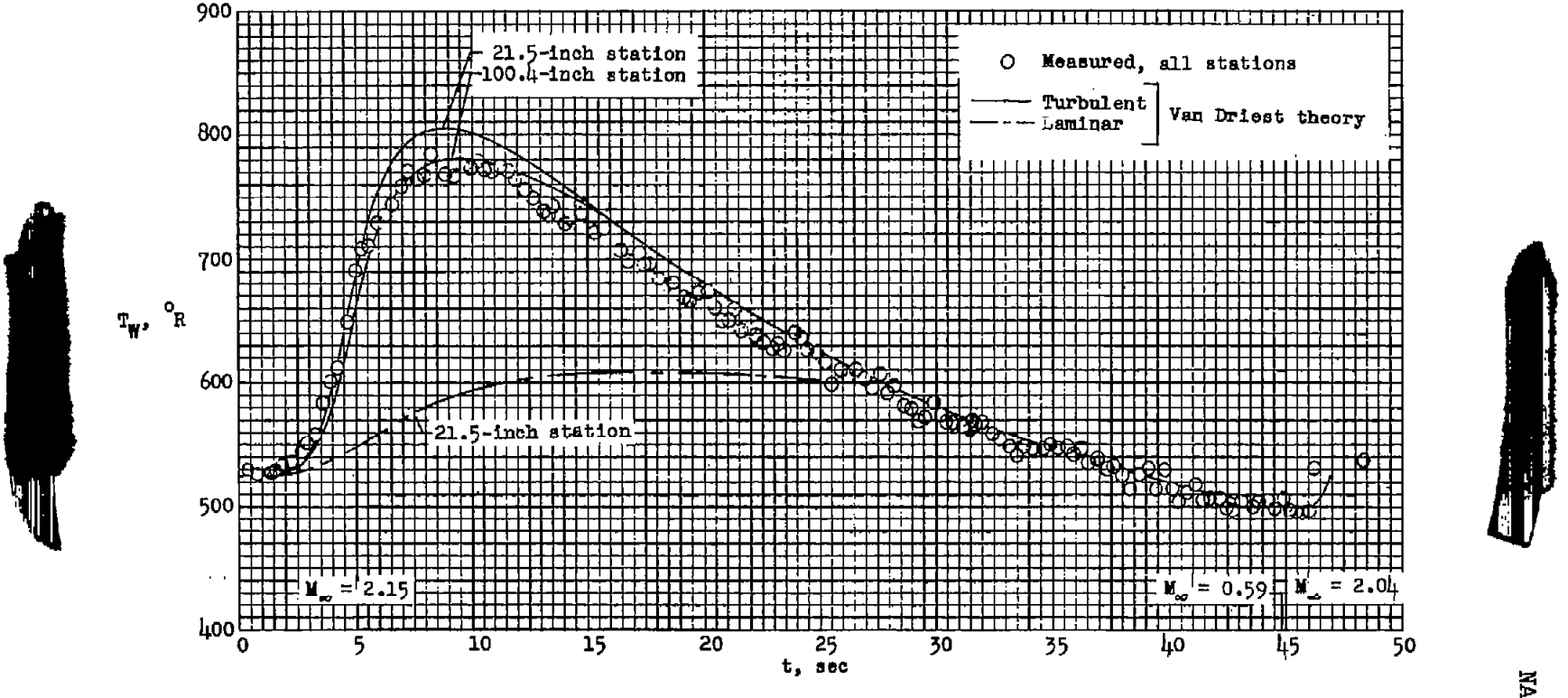

Figure 8.- Comparison of measured skin temperatures with theory.

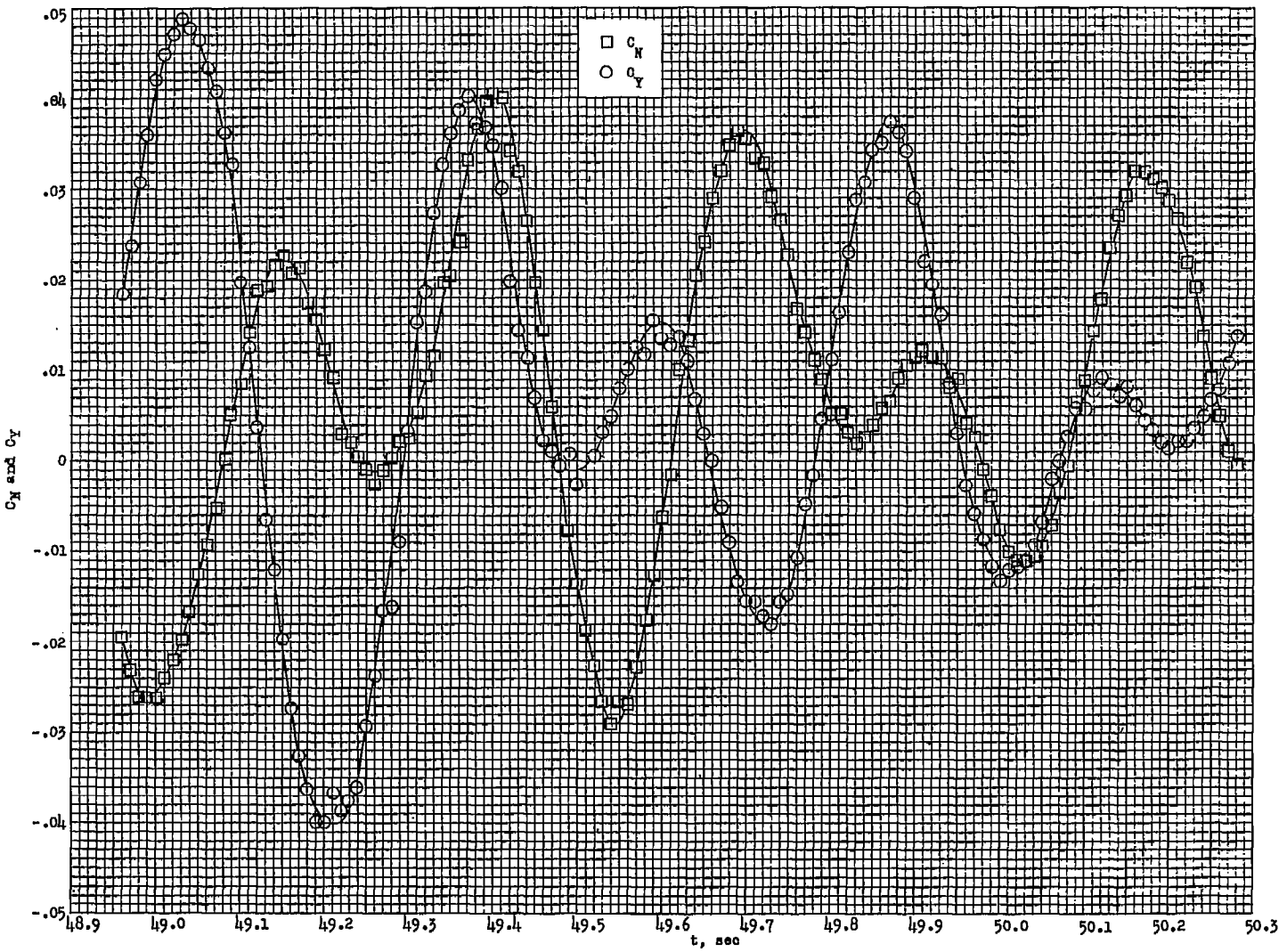

Figure 9.- Lateral- and normal-force coefficients following model disturbance.

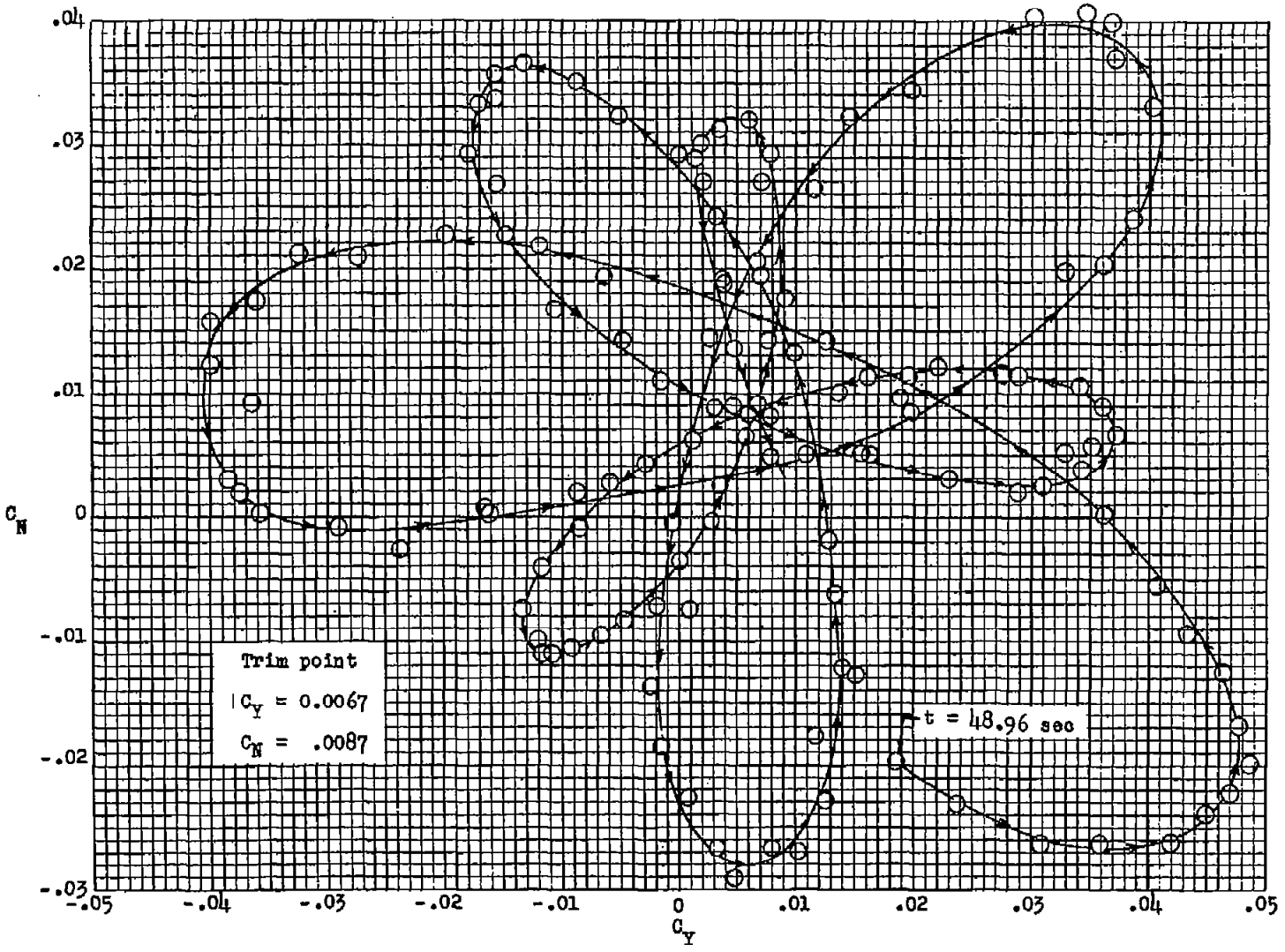

Figure 10.- Cross plot of lateral- and normal-force coefficients showing trim center.

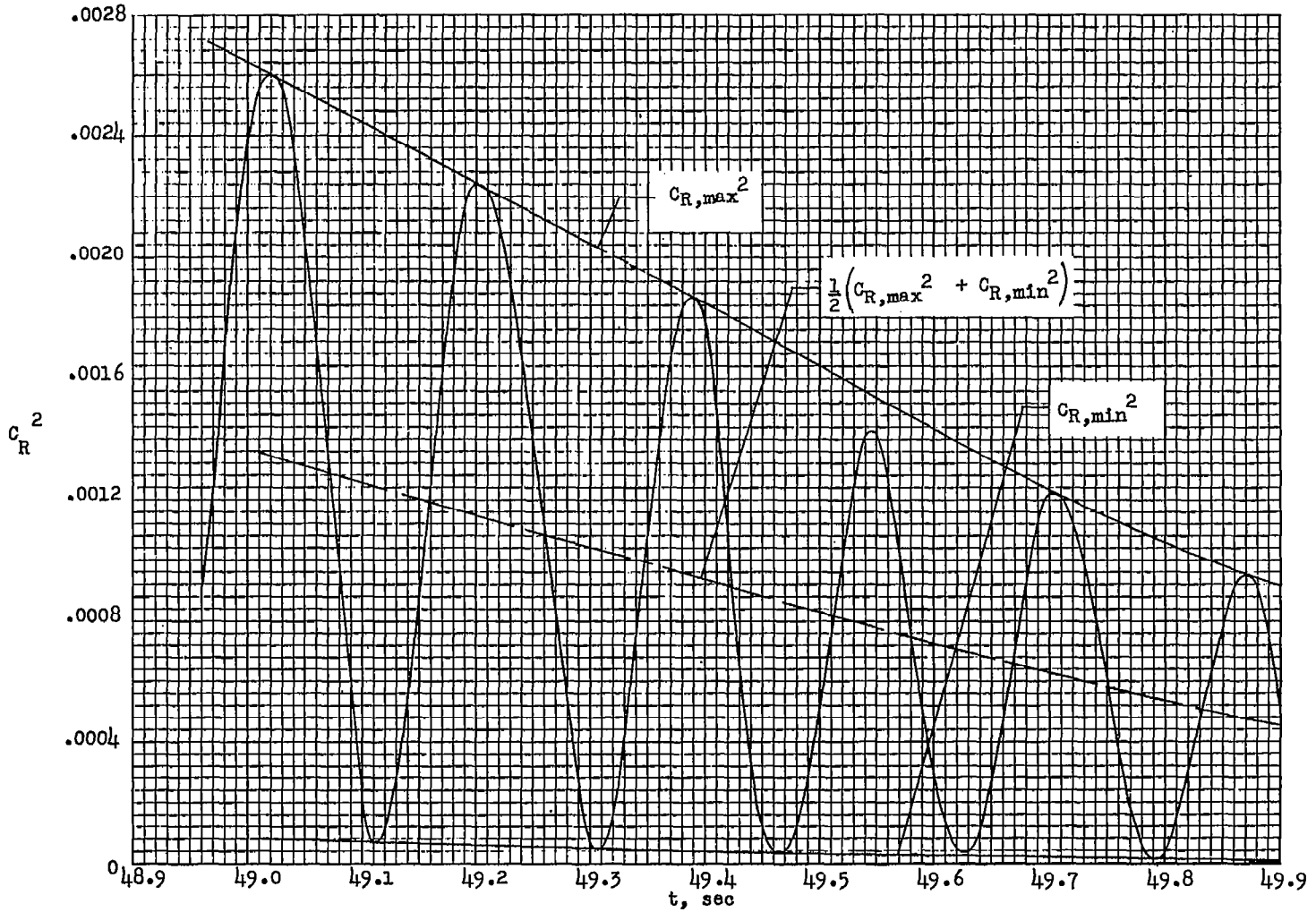

Figure 11.- Resultant of lateral- and normal-force coefficients plotted against time showing damping envelopes.

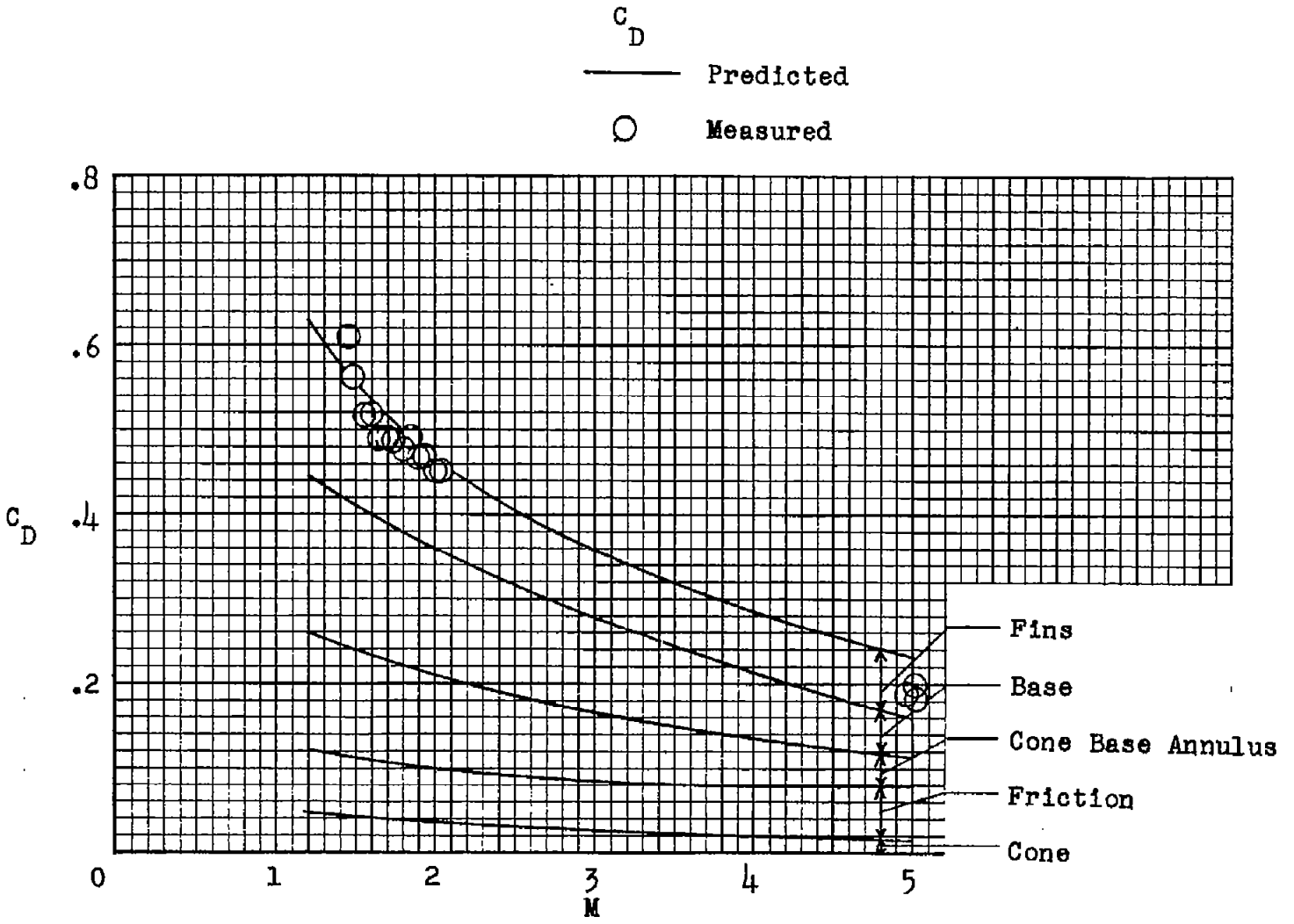

Figure 12.- Drag coefficients of model and booster.

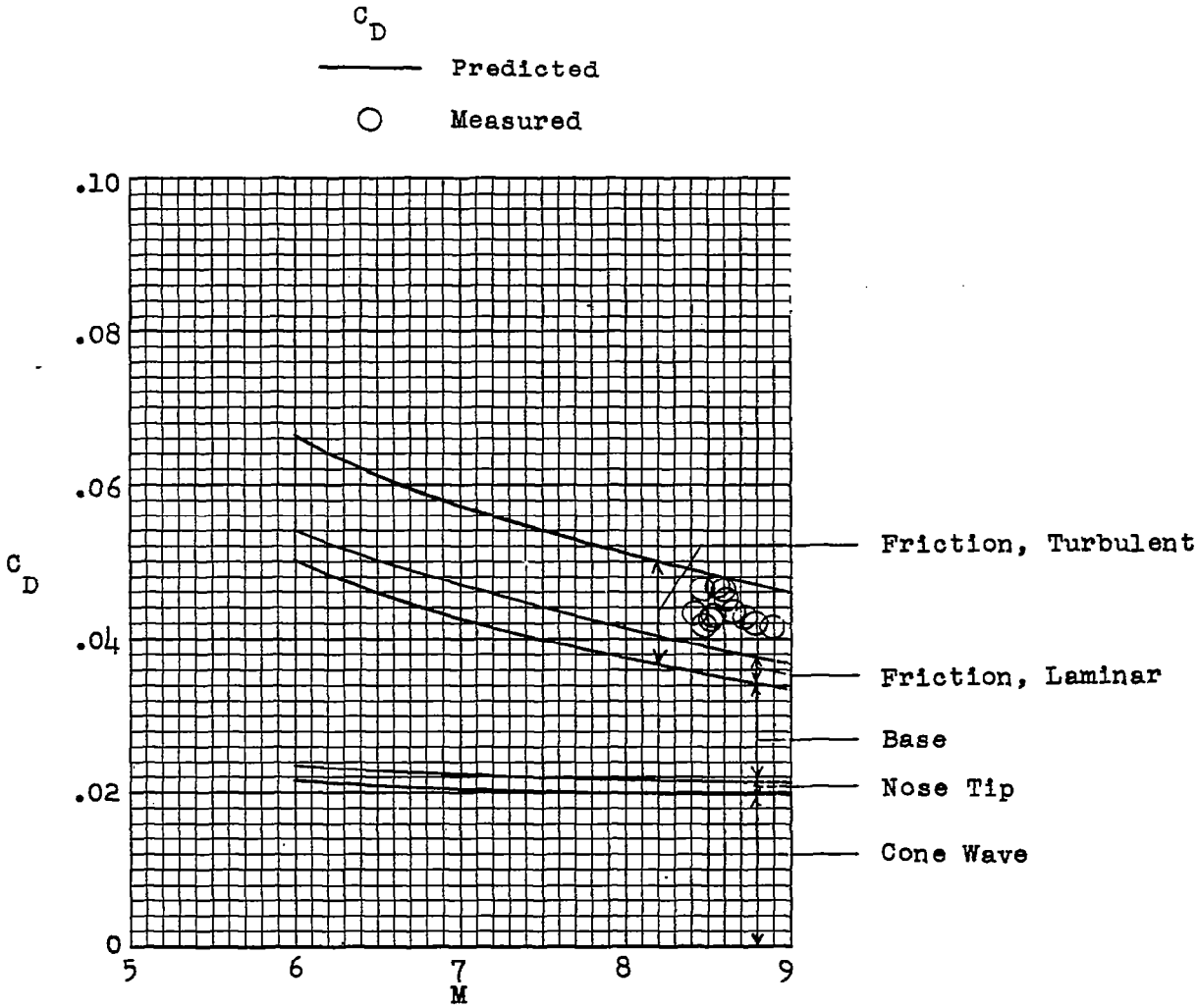

Figure 13.- Drag coefficients of model alone.

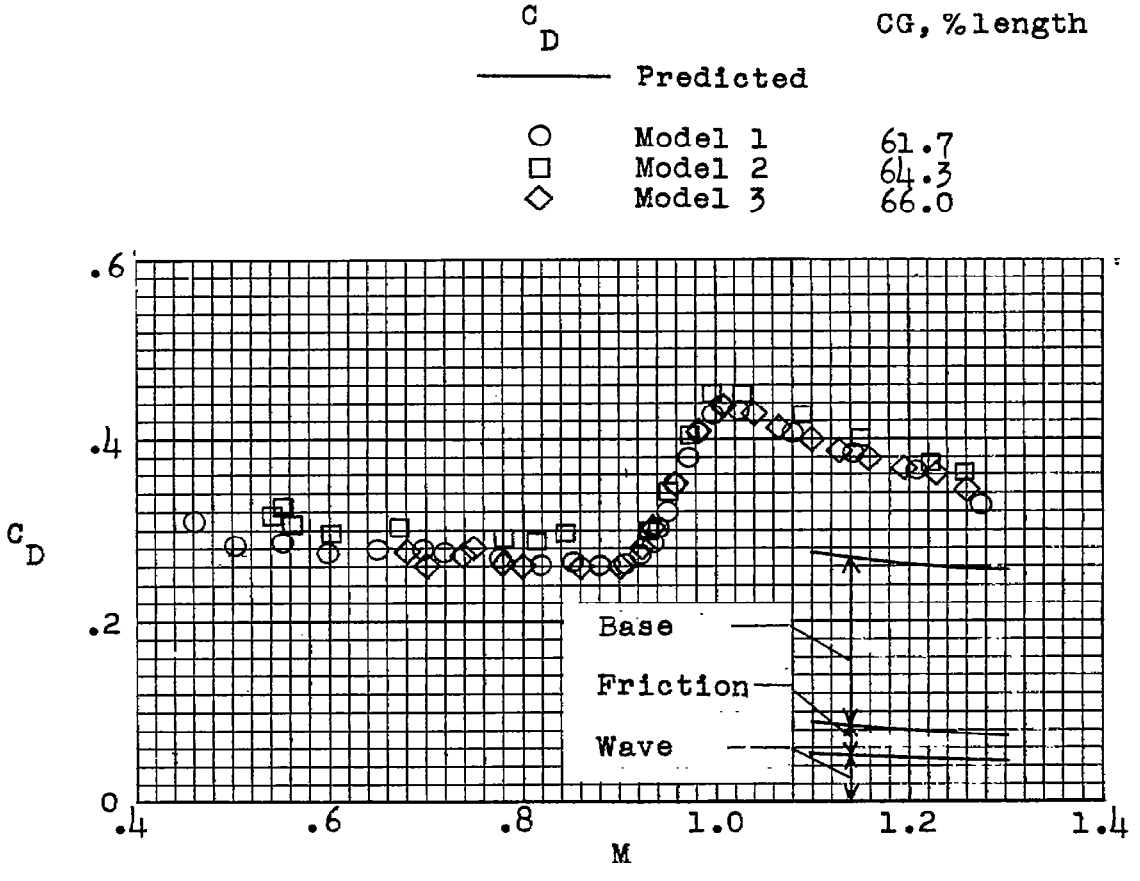

Figure 14.- Variation of drag coefficients with Mach number for helium-gun models.